ISSN 0208-7774 TRIBOLOGIA 1/2023 p. 85–97
DOI: 10.5604/01.3001.0016.2936

**Mariusz WARZECHA*, Rafał GRZEJDA****

# AN IMPROVED APPROACH IN THE APPLICATION OF AN ELASTIC-PLASTIC CONTACT FORCE MODEL IN THE MODELLING OF MULTIPLE IMPACTS

# ULEPSZONE PODEJŚCIE DO WYKORZYSTANIA ELASTO-PLASTYCZNEGO MODELU SIŁY KONTAKTU W MODELOWANIU ZDERZENIA WIELOKROTNEGO

**Key words:** multiple impact, multi-body system, elastic-plastic contact, contact force model, Finite Element Method

**Abstract:** This paper presents the modelling of a simultaneous multiple collision occurring between several bodies of a kinematic chain. An algorithm is proposed that when used with an elastoplastic contact model, allows the phenomena that can occur during a multiple-body collision to be taken into account. These phenomena include the transition of the collision state from the restitution phase directly to the compression phase or successive collisions occurring along the same normal. The proposed algorithm can be used with any elastoplastic contact model. This paper presents its use with a selected model in a three-body system. Numerical calculations based on the model have been verified using the Finite Element Method (FEM). The use of the proposed improved approach reduces the post-collision velocity prediction error by 2.34% compared to the baseline description of collisions known from the literature.

**Słowa kluczowe:** zderzenie wielokrotne, układ wieloczłonowy, kontakt sprężysto-plastyczny, model siły kontaktowej, Metoda Elementów Skończonych

**Streszczenie:** W artykule przedstawiono modelowanie symultanicznego zderzenia wielokrotnego zachodzącego pomiędzy kilkoma ciałami łańcucha kinematycznego. Zaproponowano algorytm, który wykorzystany z elasto-plastycznym modelem kontaktu pozwala na uwzględnienie zjawisk, które mogą wystąpić w trakcie zderzenia wielokrotnego. Do zjawisk tych zaliczyć można przejście stanu zderzenia z fazy restytucji bezpośrednio do fazy kompresji czy też kolejne zderzenia zachodzące wzdłuż tej samej normalnej. Zaproponowany algorytm może zostać wykorzystany z dowolnym, elasto-plastycznym modelem kontaktu. W artykule przedstawiono jego wykorzystanie z wybranym modelem w modelu składającym się z trzech ciał. Obliczenia numeryczne przeprowadzone na podstawie modelu zostały zweryfikowane za pomocą Metody Elementów Skończonych (MES). Zastosowanie zaproponowanego, ulepszonego podejścia pozwala na zmniejszenie błędu przewidywania prędkości po zderzeniu o 2.34% w porównaniu z opisem bazowym zderzenia znanym z literatury.

## INTRODUCTION

Multiple impacts are observed in various systems. Especially interesting from an engineering perspective are multi-body systems (MBS). Examples of such systems are automatic ball balancers **[L. 1]**, vibration mills **[L. 2]**, composite granular protectors **[L. 3]**, impact oscillators **[L. 4]** or hammer crushers **[L. 5]**. Furthermore, multiple impacts can be used for hard coating testing **[L. 6]**, occur in dissipative granular chains **[L. 7]**, during discrete element (DEM) simulations of sand **[L. 8**, **9]**, or multi-physical simulations that predict erosive impacts of solid particles in viscous fluids

* ORCID: 0000-0002-7417-1561, AGH University of Science and Technology, Faculty of Mechanical Engineering and Robotics, e-mail: mwarzech@agh.edu.pl, corresponding author.
** ORCID: 0000-0002-8323-1335, West Pomeranian University of Technology in Szczecin, Faculty of Mechanical Engineering and Mechatronics, e-mail: rafal.grzejda@zut.edu.pl.

**[L. 10]**. Collisions are omnipresent in various technical systems ranging from space **[L. 11]**, aircraft **[L. 12]**, and material property testing **[L. 13]** to bioengineering and marine **[L. 15**, **16]**. Therefore, the study of impact processes can be seen as a crucial problem.

When taking into account the time-resolved information about an impact, it can be divided into two phases: compression and restitution. During the compression phase, the relative velocity of the impacting bodies decreases until it reaches zero, and a restitution phase starts, in which the energy stored in local deformation is restored and causes the separation of the bodies with rebound velocity. In multiple impacts, the next compression phase starts along the same impact direction after the termination of the previous restitution phase or, as is often the case in simultaneous, multi-point impacts, even before the restitution phase ends. Because of this, modelling multiple impacts is a challenging and interesting research field **[L. 17]**.

Elastic-plastic contact force models were used to model impact in various studies. Ghaednia et al. **[L. 18]** applied the elastic-plastic contact force model to predict permanent deformation resulting from the impact of a rod with a flat surface. Other articles **[L. 19–22]** investigated phenomena observed in a chain of beads or particles. In those studies, elastic-plastic contact models were used to provide better insight into wave propagation and possible application in shock absorption. Daraio et al. **[L. 23]** also analysed energy trapping in a granular medium. The elastic-plastic contact force model was also applied to predict the coefficient of restitution **[L. 24]**. A broader overview of elastic-plastic contact force models and their applications can be found in **[L. 25**, **26]**.

Elastic-plastic contact force models have usually been developed and validated for systems consisting of two bodies. Their application to more complex systems, where simultaneous, multiple collisions can occur, poses a challenge and results in phenomena that have not been studied well. In recognising this gap, the present article attempts to identify behaviour specific to such systems and proposes an enhancement to elastic-plastic contact force models. The remainder of this paper is organised as follows. Section 2 defines in more detail the investigated problem and describes the methodology. Section 3 proposes an algorithm to enhance elastic-plastic contact force models. Section 4 presents results achieved by the application of the proposed algorithm to one of the selected models, provides a comparison with data obtained from the FEM (Finite Element Method) model, and offers a discussion, while Section 5 concludes the article.

## PROBLEM DEFINITION AND METHODOLOGY

The deformation of bodies that occurs in the vicinity of the contact point is usually divided into fully elastic, elastic-plastic, and fully plastic. Contact force models typically define separate laws for each of these regions and differentiate between the loading and unloading phases. Although these laws are different for various contact force models, the idea of switching the equations between phases is similar for all models. Therefore, without a lack of generality, we demonstrate the improvement proposed in this article using the Kogut and Etsion (KE) model as an example **[L. 27**, **28]**. The developed approach can be applied analogously to other models.

The following equations define the KE model:

$$F_n = F_{ny}(\delta^*)^{\frac{3}{2}} \text{ for } \delta^* < 1 \text{ and } \dot{\delta} > 0 \tag{1}$$

$$F_n = 1.03F_{ny}(\delta^*)^{1.425} \text{ for } 1 \leq \delta^* \leq 6 \text{ and } \dot{\delta} > 0 \tag{2}$$

$$F_n = 1.40F_{ny}(\delta^*)^{1.263} \text{ for } 6 < \delta^* \leq 110 \text{ and } \dot{\delta} > 0 \tag{3}$$

$$F_n = F_{nm}\left(\frac{\delta^* - \delta_r^*}{\delta_m^* - \delta_r^*}\right)^{n_p} \text{ for } \dot{\delta} \leq 0 \tag{4}$$

$$F_{ny} = \frac{4}{3}E^*(R^*)^{\frac{1}{2}}(\delta_y)^{\frac{3}{2}} \tag{5}$$

$$\delta_y = \left(\frac{2.8\pi K_\nu S_y}{2E^*}\right)^2 R^* \tag{6}$$

$$E^* = \left(\frac{1-\nu_1^2}{E_1} + \frac{1-\nu_2^2}{E_2}\right)^{-1} \tag{7}$$

$$R^* = \left(\frac{1}{R_1} + \frac{1}{R_2}\right)^{-1} \tag{8}$$

$$K_\nu = 0.454 + 0.41\nu \tag{9}$$

$$\delta^* = \frac{\delta}{\delta_y} \tag{10}$$

$$\delta_r^* = \delta_m^* \left(1 - \frac{1}{\left(\frac{\delta_m}{\delta_y}\right)^{0.28}}\right)\left(1 - \frac{1}{\left(\frac{\delta_m}{\delta_y}\right)^{0.69}}\right) \tag{11}$$

$$n_p = 1.5(\delta_m^*)^{-0.0331} \tag{12}$$

where: $F_n$ – normal contact force [N], $F_{nm}$ – normal contact force at the instant when unloading starts [N], $F_{ny}$ – normal contact force at the instant when the yield starts, defined by equation (5) [N], $\delta$ and $\dot{\delta}$ – deformation [m] and velocity [m/s] of contacting bodies, $\delta^*$ – deformation normalised by deformation at the instant when the yield starts, defined by equation (10) [-], $\delta_m$ – deformation at the instant when unloading starts [m] and $\delta_m^*$ deformation at the instant when unloading starts normalised by deformation at the instant when yield starts [-], $\delta_y$ – deformation at the instant when the yield starts, defined by equation (6) [m], $E_1$ and $E_2$ – Young's modulus of the body material, $E^*$ – effective Young modulus, defined by equation (7), [MPa] $\nu_1$ and $\nu_2$ – Poisson's ratio of the body material [-], $S_y$ – yield strength of the material [MPa] (if bodies are made of two different materials, $S_y$ is taken from the weaker one), $R_1$ and $R_2$ – surface curvature radius of the contacting bodies in the vicinity of the contact point [m], $R^*$ – effective surface curvature radius in the vicinity of the contact point, defined by equation (8) [m], $K_\nu$ – yield strength coefficient, defined by equation (9) [-], $\delta_r^*$ – residual deformation normalised by deformation at the instant when the yield starts, defined by equation (11) [-], $n_p$ – exponent in unloading relation, defined by equation (12), [-].

The KE model defines three relations to determine the contact force in the loading phase ($\dot{\delta} > 0$) and one for the unloading phase ($\dot{\delta} \leq 0$). It should be noted that the relations given for the loading phase do not result in a continuous contact force.

**Problem definition**

The development of published contact force models has been based on two-body systems. An impact analysed in such systems consists of the compression phase, which starts from a non-contact state, followed by the restitution phase, the end of which is unambiguous with the impact end. Nevertheless, more complex phenomena may occur in multi-body systems, reducing the contact models' prediction accuracy. Such phenomena may include switching to the compression phase during the restitution phase or starting the next collision along the same collision normal.

To illustrate potential problems which may arise during the application of the contact force model in complex systems, let us analyse collisions occurring in the system presented in **Fig. 1**. It consists of 3 balls made of X105CrMo17 stainless steel for which the following parameters were used: Young's modulus – 209 GPa, Poisson's ratio – 0.283, yield strength – 1175 MPa, density – 7.8 g/cm, and Brinell hardness – 2756.8 MPa.

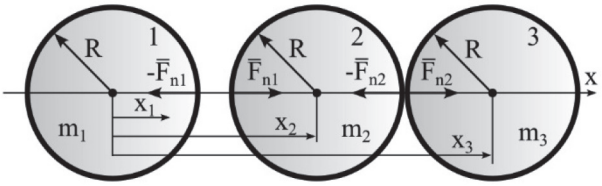


**Fig. 1. A system of three collinear balls used to illustrate potential problems arising during the application of the contact force model in a complex system; the forces $F_{n1}$ and $F_{n2}$ are a result of the boundary condition, which permits interpenetration of balls and act only when contact occurs**

Rys. 1. Układ trzech, ustawionych współosiowo kul użyty do zobrazowania problemów mogących wystąpić przy wykorzystaniu modelu siły kontaktu w złożonym systemie; siły $F_{n1}$ oraz $F_{n2}$ są rezultatem warunku brzegowego zapobiegającego wzajemnej penetracji kul i działają wyłącznie w trakcie występowania kontaktu

Neglecting all forces except those resulting from frictionless contact, the equations of motion for the system can be written as follows:

$$m_1\ddot{x}_1 = -F_{n1} \tag{13}$$

$$m_2\ddot{x}_2 = F_{n1} - F_{n2} \tag{14}$$

$$m_3\ddot{x}_3 = F_{n2} \tag{15}$$

$$\delta_1 = \max\{x_1 - x_2 - 2R, 0\} \tag{16}$$

$$\delta_2 = \max\{x_2 - x_3 - 2R, 0\} \tag{17}$$

$$\dot{\delta}_1 = \dot{x}_1 - \dot{x}_2 \tag{18}$$

$$\dot{\delta}_2 = \dot{x}_2 - \dot{x}_3 \tag{19}$$

where: $m_1$, $m_2$, $m_3$ are ball masses, $x_1$, $x_2$, $x_3$ are coordinates that give the ball positions as shown in **Fig. 1**, $F_{n1}$, $F_{n2}$ are contact forces resulting from equations (1)-(12), $\delta_1$, $\delta_2$ are local deformations of colliding balls and $\delta_1$, $\delta_2$ their relative velocity.

Equations (13) – (19) form a second-order nonlinear differential equations system. This system was solved numerically using a script developed in Python. The script was based on two established libraries: NumPy and SciPy, and used to integrate the explicit Runge-Kutta method of order 4(5) with a time step equal to 10 s. The initial conditions were as follows: $x_1^0 = 0$ m, $x_2^0 = 20.07 \cdot 10^{-3}$ m, $x_3^0 = 40.07 \cdot 10^{-3}$ m, $\dot{x}_1^0 = 3$ m/s, $\dot{x}_2^0 = 1$ m/s, $\dot{x}_3^0 = 0$ m/s. Such values were chosen to illustrate a complex case in which the compression phase starts during the restitution phase.

**Fig. 2** shows the impact force resulting from the collision of balls 2 and 3 for the system and the initial conditions described above. The force was presented as a function of time and local deformation to better present the behaviour of the contact force model. It can be seen that the collision force and local deformation increase until the relative velocity drops to 0 and the force and deformation reach the local maximum. The restitution phase starts at this point, marked as 1 in **Fig. 2**. Before the collision between balls 2 and 3 ceases, ball 1 impacts ball 2, which causes the collision between balls 2 and 3 to switch to the compression phase. This point is marked as 2 in **Fig. 2**. Because the initial velocity of ball 1 was substantially higher than the initial velocity of ball 2, the maximum contact force and local deformation reached higher values marked by 3 in **Fig. 2**. It seems logical that the discontinuity at point 2 has no physical justification. It is a consequence of the inability of the contact force model to take into account the plastic deformation which occurred in the previous collision or compression phase. Therefore, when the compression phase starts during the restitution phase, the model switches to the loading relation, which, consequently, creates visible discontinuity and decreases the ability of the contact model to predict the impact quantities, especially the rebound velocity, properly.

The second identified problem was related to modelling multiple collisions occurring along the same direction. The models available in the literature **[L. 18**, **24**, **27**, **29**, **30]** predict the results of the first collision quite well but cannot incorporate changes related to plastic deformation in subsequent impacts, increasing the model error. In order to demonstrate such a case, the system given by Equations (13) – (19) was used with the following initial conditions: $x_1^0 = 0$ m, $x_2^0 = 20.06 \cdot 10^{-3}$ m, $x_3^0 = 40.06 \cdot 10^{-3}$ m, $\dot{x}_1^0 = 1.5$ m/s, $\dot{x}_2^0 = 1$ m/s, $\dot{x}_3^0 = 0$ m/s. It is necessary to mention that, in this case, the numerical simulation was stopped after the termination of the first collision, and an adjustment to the system state was introduced to include the permanent deformation resulting from the first impact. Otherwise, the simulation would result in a result with no sense, as just after the impact termination, the system state would indicate deformation equal to the plastic deformation and automatically switch to the collision state. The simulation result is shown in **Fig. 3**. The left plot,

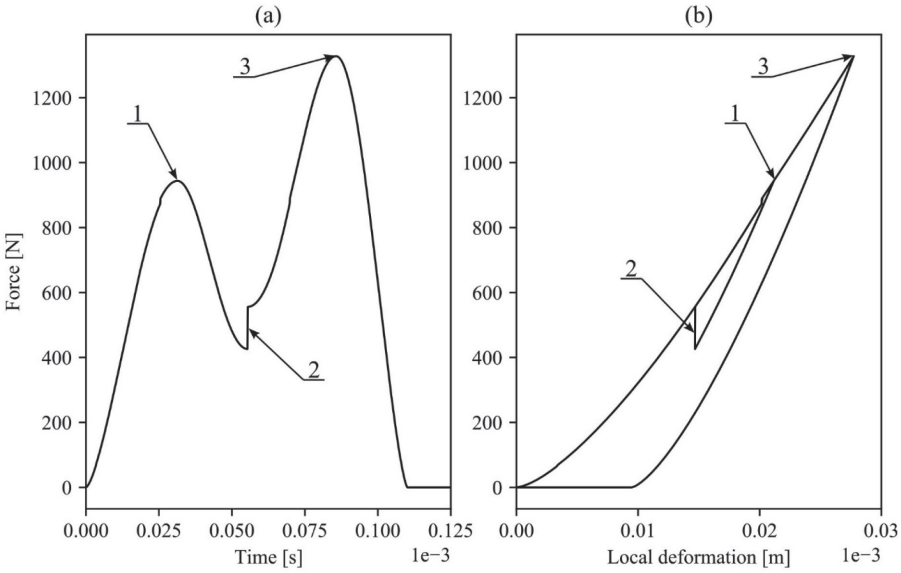


**Fig. 2. Impact force resulting from the collision of balls 2 and 3 for the initial conditions: $x_1^0 = 0$ m, $x_2^0 = 20.07 \cdot 10^{-3}$ m, $x_3^0 = 40.07 \cdot 10^{-3}$ m, $\dot{x}_1^0 = 3$ m/s, $\dot{x}_2^0 = 1$ m/s, $\dot{x}_3^0 = 0$ m/s; (a) plotted as a function of time and (b) plotted as a function of local deformation**

Rys. 2. Siła zderzenia powstająca w trakcie zderzenia kul 2 oraz 3 dla następujących warunków brzegowych: $x_1^0 = 0$ m, $x_2^0 = 20{,}07 \cdot 10^{-3}$ m, $x_3^0 = 40{,}07 \cdot 10^{-3}$ m, $\dot{x}_1^0 = 3$ m/s, $\dot{x}_2^0 = 1$ m/s, $\dot{x}_3^0 = 0$ m/s; (a) wykres w funkcji czasu i (b) wykres w funkcji lokalnego odkształcenia

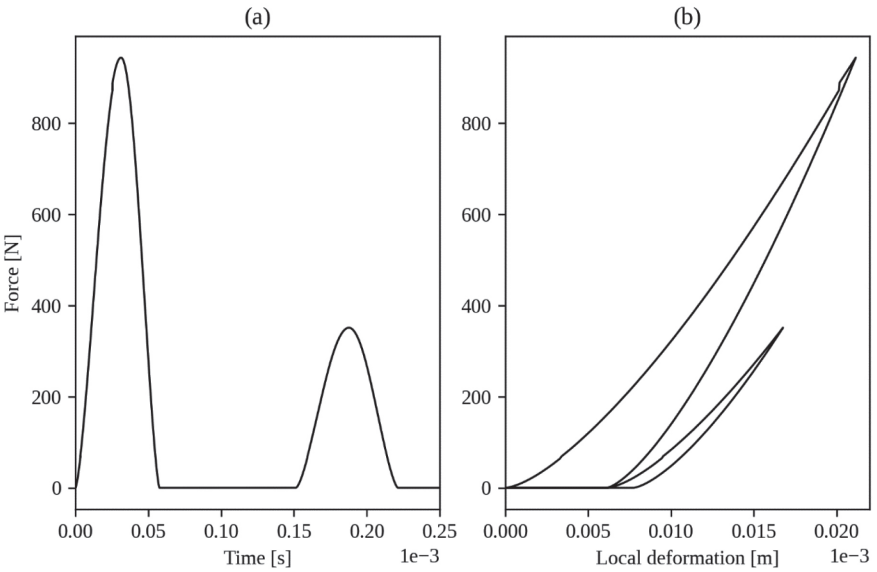


**Fig. 3. Impact force resulting from the collision of balls 2 and 3 for the initial conditions: $x_1^0 = 0$ m, $x_2^0 = 20.06 \cdot 10^{-3}$ m, $x_3^0 = 40.06 \cdot 10^{-3}$ m, $\dot{x}_1^0 = 1.5$ m/s, $\dot{x}_2^0 = 1$ m/s, $\dot{x}_3^0 = 0$ m/s; (a) plotted as a function of time and (b) plotted as a function of local deformation**

Rys. 3. Siła zderzenia powstająca w trakcie zderzenia kul 2 oraz 3 dla następujących warunków brzegowych: $x_1^0 = 0$ m, $x_2^0 = 20{,}06 \cdot 10^{-3}$ m, $x_3^0 = 40{,}06 \cdot 10^{-3}$ m, $\dot{x}_1^0 = 1{,}5$ m/s, $\dot{x}_2^0 = 1$ m/s, $\dot{x}_3^0 = 0$ m/s; (a) wykres w funkcji czasu i (b) wykres w funkcji lokalnego odkształcenia

described as (a), gives the time history of the impact force between balls 2 and 3. Due to manual modification of the system state, both collisions are separated in time, and it seems reasonable to include this functionality in model implementation. Another observation can be made in the right plot, described as (b), which shows the impact force as a function of local deformation. The curves

for both collisions are separate, whereas it seems reasonable to expect that the loading phase of the next collision will somewhat follow the unloading curve of the previous collision.

The solution to the described problems will be proposed in the following sections.

### Validation methodology

The elastic-plastic contact force models available in the literature have mainly been developed and validated using data generated by models developed with the Finite Element Method (FEM). This approach is commonly accepted as the FEM method, which has been proven to deliver reliable results within the scope of contact modelling; it has been demonstrated by indentation and flattening tests using various materials and geometries **[L. 31–35]**. Therefore, we developed the FEM model of the analysed system to have a reference for the proposed improvements and to check their impact on the obtained results, including the assessment of error reduction achieved by the proposed algorithm.

The developed FEM model was based on the open-source CODE-ASTER 14.6 solver **[L. 36]**. It allows both static and dynamic nonlinear analysis. In this case, the routine DYNA_NON_LINE was used to analyse the system's dynamic behaviour. Due to the axial symmetry of the system, the elements named AXIS were used. In order to generate the mesh of the half-circle geometry, GMSH **[L. 37]** was used. The element size in the contact area was determined iteratively by subsequent simulation and reduction of the element size to the point when the change in stresses was less than 1%. The final element size in the contact area was set to 0.0166 mm and was constant at a distance smaller than 1.673 mm from the initial contact point. The elements with nodes with a distance greater than 1.673 mm from the initial contact point gradually increased in size until reaching 1mm. The generated mesh is shown in **Fig. 4**.

The model created in CODE-ASTER consisted of three identical ball meshes. This was achieved by copying the mesh generated in GMSH and translating it by the distance necessary to obtain the initial positions. The contact used the discrete formulation. The initial time step was set to 3.25 μs, but an adaptive time step was used so that the time step was automatically reduced when the model could not achieve congruence. Post-processing was performed using Python scripts operating on concepts stored during simulation. This is a very convenient solution as CODE-ASTER uses Python scripting language for simulation definition files.

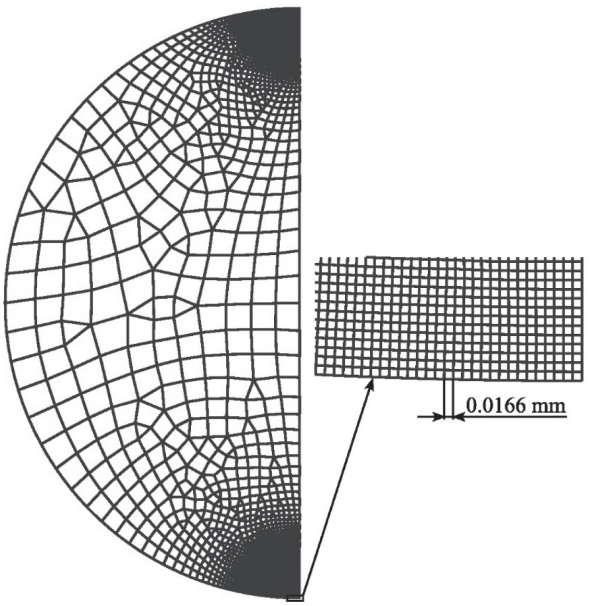


**Fig. 4. Mesh used for the Finite Element Model**
Rys. 4. Siatka elementów skończonych wykorzystana w analizie Metodą Elementów Skończonych

## PROPOSED ALGORITHM

As discussed previously, the application of contact force models in the simulation of impacts in multi-body systems may result in errors related to phenomena such as switching the collision state to compression directly from the restitution phase or multiple impacts occurring along the same impact normal. To reduce this error, we have proposed an algorithm that added additional features to the contact force model. This algorithm can be used to enhance any elastic-plastic contact force model available in the literature.

The algorithm is presented in graphical form as the block diagram shown in **Fig. 5**. It extends the functionality of the contact model by the ability to detect the switch to compression from the restitution phase (or, in other words, from unloading directly to loading) and allows detection of previous impacts along the same normal. In the former case, the algorithm uses the modified relation for the loading phase to include part of the plastic deformation, which occurred during the compression phase. This approach seems to be reasonable and ensures that the contact force is

continuous. In the latter case, the permanent plastic deformation resulting from previous collisions is stored in the memory and used to modify the model input deformation (in this article Eqs. 16 and 17). Moreover, if the permanent plastic deformation is nonzero at the start of the collision, the algorithm uses the unloading relation of the contact model (in this case, Eq. 4) until the deformation reaches and exceeds the value achieved in the previous collision.

It is important to reiterate that the algorithm can be used as a 'wrapper', adding functionality to any elastic-plastic contact force model. Furthermore, the implementation can add these features as an option, which can be switched on and off depending on the investigated model. This enhances the reusability of the code.

In order to investigate the correctness of the proposed algorithm; it was implemented as an enhancement to the Kogut and Etsion contact force model. The implementation was performed in the Python programming language. The results obtained are presented in the following section.

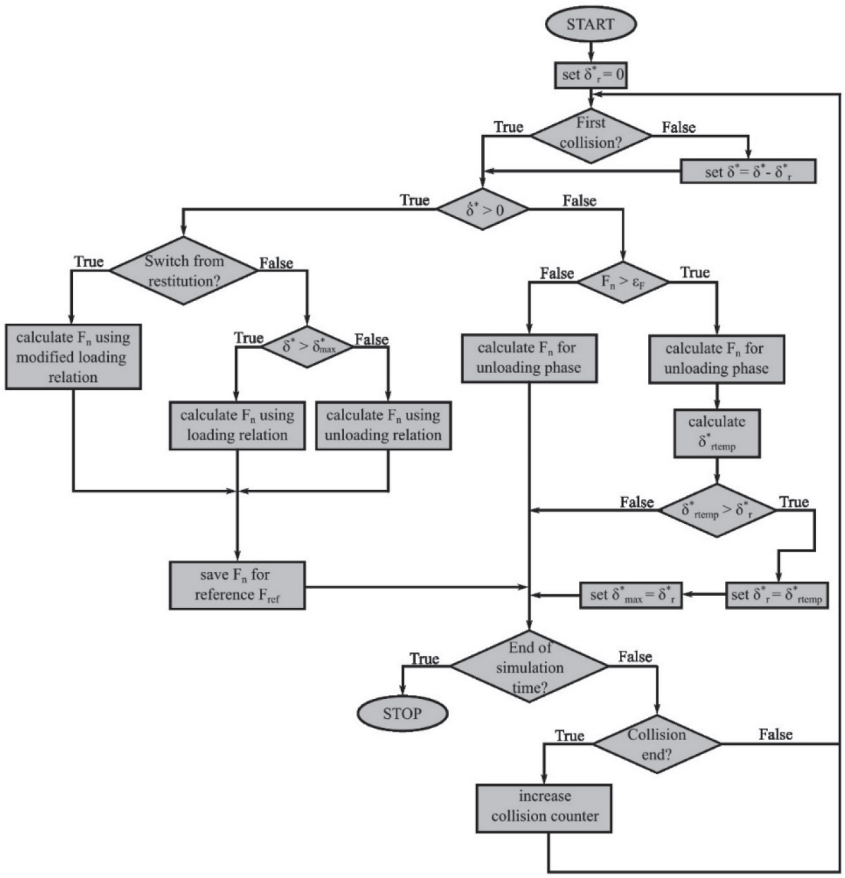


**Fig. 5. Block diagram of the proposed algorithm**
Rys. 5. Schemat blokowy zaproponowanego algorytmu

## RESULTS AND DISCUSSION

The algorithm proposed in the previous section is intended to improve the performance of the contact force model in modelling multiple impacts that occur during the analysis of multi-body systems. This improvement is achieved by (a) removing the discontinuity that occurs during the switch from restitution to the compression phase and (b) taking into account the permanent plastic deformation from previous impacts. The methodology of the algorithm is general and can be applied to any contact force model that expresses energy dissipation by plastic deformation occurring in the impacting bodies in the vicinity of the contact point. Therefore, to show that the algorithm can be correctly implemented, we selected one contact force model as an example. Of course, the error reduction achieved will vary depending on the contact model, and its broader study poses an interesting problem, but it is outside the scope of this article. This section presents results obtained

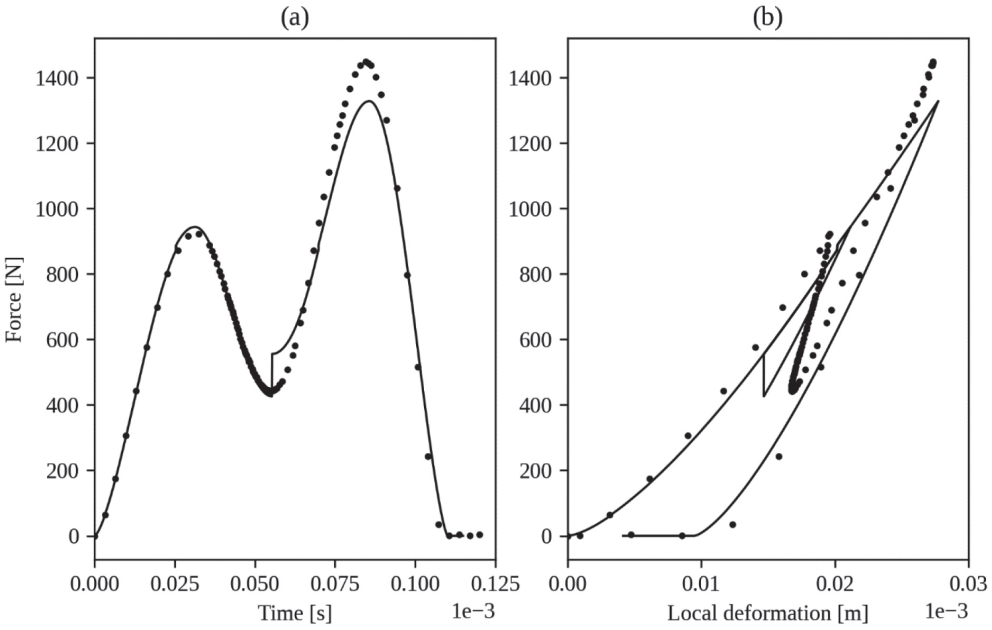


**Fig. 6. Impact force resulting from the collision of balls 2 and 3 for the initial conditions: $x_1^0 = 0$ m, $x_2^0 = 20.07 \cdot 10^{-3}$ m, $x_3^0 = 40.07 \cdot 10^{-3}$ m, $\dot{x}_1^0 = 3$ m/s, $\dot{x}_2^0 = 1$ m/s, $\dot{x}_3^0 = 0$ m/s for a basic contact force model; dots represent values obtained from the FEM simulation (a) plotted as a function of time and (b) plotted as a function of local deformation**

Rys. 6. Siła zderzenia powstająca w trakcie zderzenia kul 2 oraz 3 dla następujących warunków brzegowych: $x_1^0 = 0$ m, $x_2^0 = 20{,}07 \cdot 10^{-3}$ m, $x_3^0 = 40{,}07 \cdot 10^{-3}$ m, $\dot{x}_1^0 = 3$ m/s, $\dot{x}_2^0 = 1$ m/s, $\dot{x}_3^0 = 0$ m/s dla wyjściowego modelu kontaktu; kropki reprezentują wartości referencyjne otrzymane z symulacji MES (a) wykres w funkcji czasu i (b) wykres w funkcji lokalnego odkształcenia

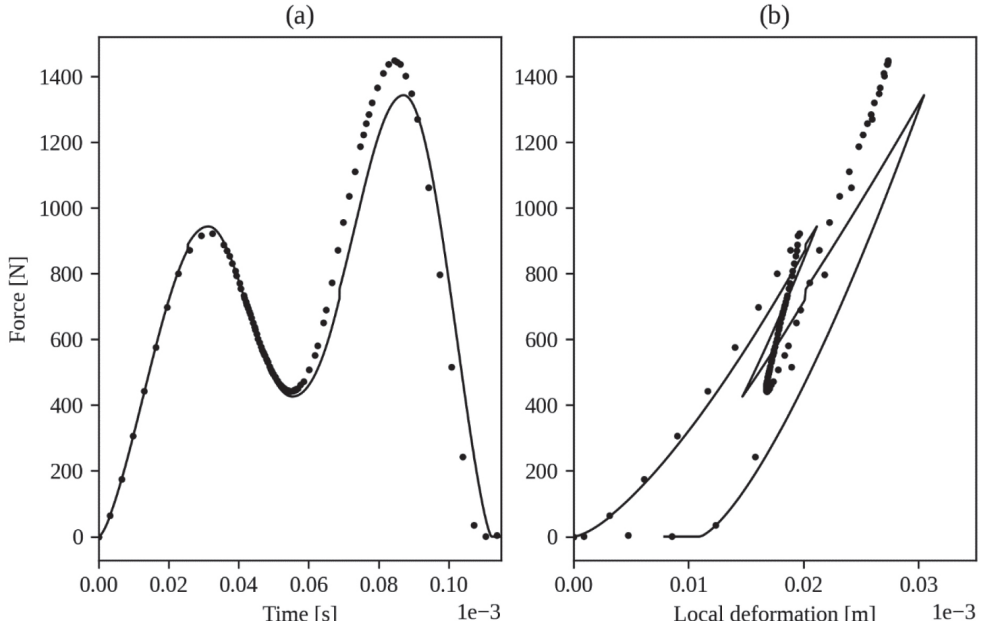


**Fig. 7. Impact force resulting from the collision of balls 2 and 3 for the initial conditions: $x_1^0 = 0$ m, $x_2^0 = 20.07 \cdot 10^{-3}$ m, $x_3^0 = 40.07 \cdot 10^{-3}$ m, $\dot{x}_1^0 = 3$ m/s, $\dot{x}_2^0 = 1$ m/s, $\dot{x}_3^0 = 0$ m/s for an enhanced contact force model; dots represent values obtained from the FEM simulation (a) plotted as a function of time and (b) plotted as a function of local deformation**

Rys. 7. Siła zderzenia powstająca w trakcie zderzenia kuli 2 oraz 3 dla następujących warunków brzegowych: $x_1^0 = 0$ m, $x_2^0 = 20{,}07 \cdot 10^{-3}$ m, $x_3^0 = 40{,}07 \cdot 10^{-3}$ m, $\dot{x}_1^0 = 3$ m/s, $\dot{x}_2^0 = 1$ m/s, $\dot{x}_3^0 = 0$ m/s dla modelu kontaktu z ulepszoną implementacją zaproponowaną w artykule; kropki reprezentują wartości referencyjne otrzymane z symulacji MES (a) wykres w funkcji czasu i (b) wykres w funkcji lokalnego odkształcenia

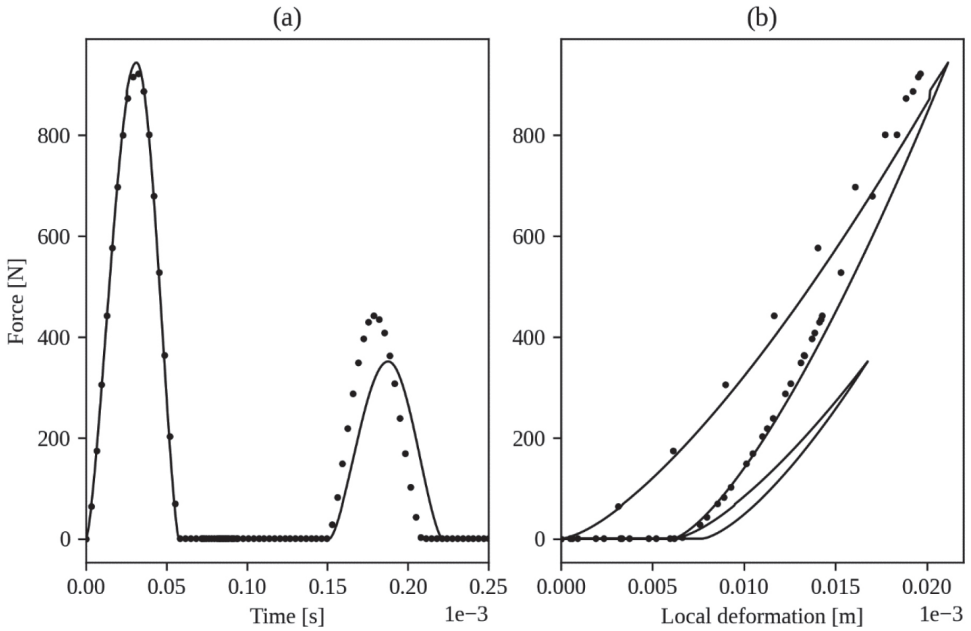


**Fig. 8. Impact force resulting from the collision of balls 2 and 3 for the initial conditions: $x_1^0 = 0$ m, $x_2^0 = 20.06 \cdot 10^{-3}$ m, $x_3^0 = 40.06 \cdot 10^{-3}$ m, $\dot{x}_1^0 = 1.5$ m/s, $\dot{x}_2^0 = 1$ m/s, $\dot{x}_3^0 = 0$ m/s for a basic contact force model, dots represent values obtained from the FEM simulation; (a) plotted as a function of time and (b) plotted as a function of local deformation**

Rys. 8. Siła zderzenia powstająca w trakcie zderzenia kuli 2 oraz 3 dla następujących warunków brzegowych: $x_1^0 = 0$ m, $x_2^0 = 20{,}06 \cdot 10^{-3}$ m, $x_3^0 = 40{,}06 \cdot 10^{-3}$ m, $\dot{x}_1^0 = 1{,}5$ m/s, $\dot{x}_2^0 = 1$ m/s, $\dot{x}_3^0 = 0$ m/s dla wyjściowego modelu kontaktu; kropki reprezentują wartości referencyjne otrzymane z symulacji MES (a) wykres w funkcji czasu i (b) wykres w funkcji lokalnego odkształcenia

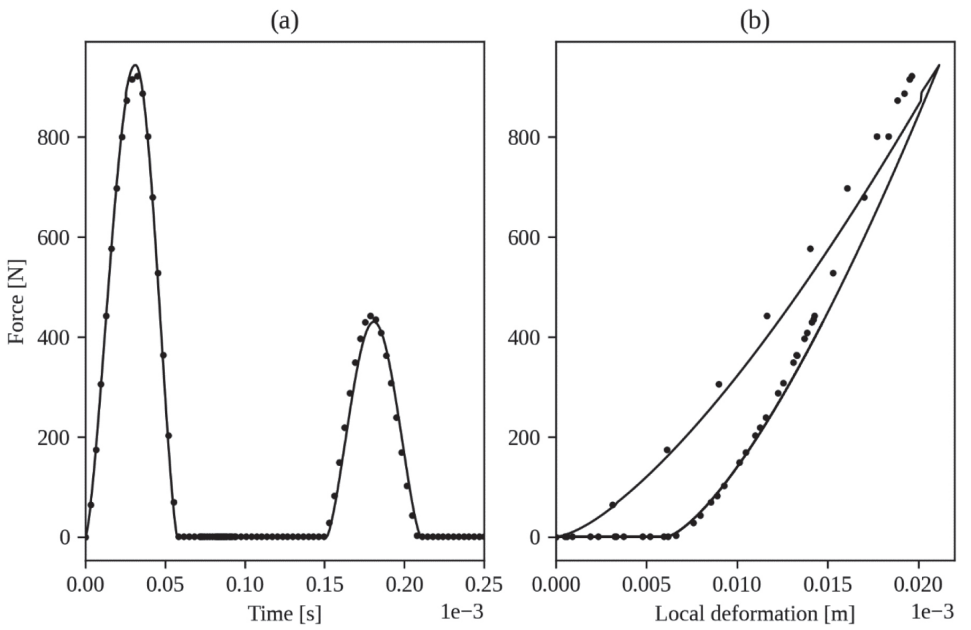


**Fig. 9. Impact force resulting from the collision of balls 2 and 3 for the initial conditions: $x_1^0 = 0$ m, $x_2^0 = 20.06 \cdot 10^{-3}$ m, $x_3^0 = 40.06 \cdot 10^{-3}$ m, $\dot{x}_1^0 = 1.5$ m/s, $\dot{x}_2^0 = 1$ m/s, $\dot{x}_3^0 = 0$ m/s for an enhanced contact force model, the dots represent the values obtained from the FEM simulation; (a) plotted as a function of time and (b) plotted as a function of local deformation**

Rys. 9. Siła zderzenia powstająca w trakcie zderzenia kuli 2 oraz 3 dla następujących warunków brzegowych: $x_1^0 = 0$ m, $x_2^0 = 20{,}06 \cdot 10^{-3}$ m, $x_3^0 = 40{,}06 \cdot 10^{-3}$ m, $\dot{x}_1^0 = 1{,}5$ m/s, $\dot{x}_2^0 = 1$ m/s, $\dot{x}_3^0 = 0$ m/s dla modelu kontaktu z ulepszoną implementacją zaproponowaną w artykule; kropki reprezentują wartości referencyjne otrzymane z symulacji MES (a) wykres w funkcji czasu i (b) wykres w funkcji lokalnego odkształcenia

by enhancing the model proposed by Kogut and Etsion used to simulate impacts in the system presented in **Fig. 1** for different initial conditions. These results were compared with those obtained from the FEM model described in Section 2.2.

**Fig. 6** and **Fig. 7** illustrate the impact force between balls 2 and 3 for the initial conditions: $x_1^0 = 0$, $x_2^0 = 20.07 \cdot 10^{-3}$ m, $x_3^0 = 40.07 \cdot 10^{-3}$ m, $\dot{x}_1^0 = 3$ m/s, $\dot{x}_2^0 = 1$ m/s, $\dot{x}_3^0 = 0$ m/s.

The impact force was plotted as a function of time and local deformation. The dots represent values obtained from the FEM analysis. A comparison of both **Figures** illustrated the correct elimination of the discontinuity resulting from the switch from restitution to the compression phase, plotted in **Fig. 6** as a vertical line. This vertical line is not present in **Fig. 7**, where the curve representing the impact force is continuous.

An analogous comparison is presented in **Fig. 8** and **Fig. 9** for the initial conditions: $x_1^0 = 0$ m, $x_2^0 = 20.06 \cdot 10^{-3}$ m, $x_3^0 = 40.06 \cdot 10^{-3}$ m, $\dot{x}_1^0 = 1.5$ m/s, $\dot{x}_2^0 = 1$ m/s, $\dot{x}_3^0 = 0$ m/s. In this case, there were two subsequent impacts between balls 2 and 3. It should be noted that the results obtained for the basic contact force model for these initial conditions resulted from two steps. After the first impact between balls 2 and 3 ended, the numerical simulation was stopped, and the system's state was manually adjusted to include permanent local deformations. Then, in the second step, the simulation was run until the end of the time limit. Such a modification was necessary because the results contained impacts that should not occur without it. It improved the output of the basic model, but without it, the comparison would not be possible, and, as can be observed in **Fig. 9**, the enhanced model still offered better results. Inspection of **Fig. 9** reveals that the contact force was better fitted to the FEM data and, which is especially visible in the curves plotted as a function of local deformation, the second impact force followed the unloading curve from the previous collision, contrary to the basic model shown in **Fig. 8**, where curves for both collisions are separate.

The ability to predict the post-impact velocities is crucial from the perspective of the multi-body simulation accuracy. In order to demonstrate how the velocities may have been affected by the enhancement of the contact force model, the results obtained during the simulations conducted are presented in **Tables 1** and **2**. The analysis of both tables demonstrates that the proposed algorithm

**Table 1. Post-impact velocities for balls 2 and 3 resulting from the basic contact force model, enhanced contact force model and FEM analysis; simulation for the initial conditions: $x_1^0 = 0$ m, $x_2^0 = 20.07 \cdot 10^{-3}$ m, $x_3^0 = 40.07 \cdot 10^{-3}$ m, $\dot{x}_1^0 = 3$ m/s, $\dot{x}_2^0 = 1$ m/s, $\dot{x}_3^0 = 0$ m/s**

Tabela 1. Prędkości kul 2 oraz 3 po zakończeniu zderzenia dla wyjściowego modelu kontaktu, jego ulepszonej implementacji zaproponowanej w artykule oraz modelu MES; symulacja dla warunków początkowych: $x_1^0 = 0$ m, $x_2^0 = 20{,}07 \cdot 10^{-3}$ m, $x_3^0 = 40{,}07 \cdot 10^{-3}$ m, $\dot{x}_1^0 = 3$ m/s, $\dot{x}_2^0 = 1$ m/s, $\dot{x}_3^0 = 0$ m/s

| Ball number | Post-impact velocity [m/s] | | | Error [%] | |
|---|---|---|---|---|---|
| | Basic model | Enhanced model | FEM | Basic model | Enhanced model |
| 2 | 0.94188 | 0.92441 | 0.91398 | -3.05 | -1.14 |
| 3 | 1.34048 | 1.35795 | 1.36217 | 1.59 | 0.31 |

**Table 2. Post-impact velocities for balls 2 and 3 resulting from the basic contact force model, enhanced contact force model, and FEM analysis; simulation for the initial conditions: $x_1^0 = 0$ m, $x_2^0 = 20.07 \cdot 10^{-3}$ m, $x_3^0 = 40.07 \cdot 10^{-3}$ m, $\dot{x}_1^0 = 3$ m/s, $\dot{x}_2^0 = 1$ m/s, $\dot{x}_3^0 = 0$ m/s**

Tabela 2. Prędkości kul 2 oraz 3 po zakończeniu zderzenia dla wyjściowego modelu kontaktu, jego ulepszonej implementacji zaproponowanej w artykule oraz modelu MES; symulacja dla warunków początkowych: $x_1^0 = 0$ m, $x_2^0 = 20{,}07 \cdot 10^{-3}$ m, $x_3^0 = 40{,}07 \cdot 10^{-3}$ m, $\dot{x}_1^0 = 3$ m/s, $\dot{x}_2^0 = 1$ m/s, $\dot{x}_3^0 = 0$ m/s

| Ball number | Post-impact velocity [m/s] | | | Error [%] | |
|---|---|---|---|---|---|
| | Basic model | Enhanced model | FEM | Basic model | Enhanced model |
| 2 | 1.29691 | 1.25946 | 1.26341 | -2.65 | 0.31 |
| 3 | 2.40896 | 2.41681 | 2.44515 | 1.48 | 1.16 |

allows a significant reduction of error, which is especially crucial in multiple impact cases, where it stacks during subsequent collisions. However, it should be noted that, for proper assessment of the error reduction, a substantially broader analysis must be conducted, which is outside the scope of this paper.

## CONCLUSIONS

The article has proposed enhancing an elastic-plastic contact force model, which should improve its accuracy in modelling multiple impacts. The proposed enhancement is focused on two phenomena: switching the impact state directly from restitution to the compression phase and multiple impacts occurring along the same impact normal and causing permanent plastic deformation. The algorithm was used to enhance one selected contact force model, and it has been shown that it can be correctly applied to achieve the expected outcomes. The results obtained were validated with the FEM model and showed that the enhanced model allowed a reduction of the velocity prediction error by up to 2.34%. This value is obviously only indicative because the investigated system was relatively simple (only three bodies), and the enhancement was applied only to one model. This problem will be addressed in future studies, where more complex systems will be analysed using different elastic-plastic contact force models, as the proposed algorithm can be used with any such model. It should be expected that the gains resulting from the enhancement will be more significant in such systems. Although the proposed algorithm offers an improvement, it must also be noted that its implementation increases the computational cost of the model. In the analysed cases, this increase was almost non-existent, but more complex systems may be influenced on a level hard to predict because of the high level of problem non-linearity. Implementing the proposed algorithm in the PROJECT CHRONO engine has been planned to study this aspect better. Studies performed with such an implementation will allow the collection of data from larger systems and a better assessment of the algorithm's impact on performance. This data, combined with a broader study of error reduction, will allow the potential user to make better judgments on possible application cases.

**Acknowledgement**: The authors acknowledge the financial support of AGH University of Science and Technology, project No. 16.16.130.942.

## REFERENCES

1. Michalczyk J., Pakuła S.: Phase control of the transient resonance of the automatic ball balancer, Mech. Syst. Signal Process., vol. 72–73, pp. 254–265, May 2016, doi: 10.1016/j.ymssp.2015.11.001.
2. Cieplok G., Piekaj P.: Movement properties of antiresonance vibration mill with symmetrical Construction, Vib. Phys. Syst., vol. 31, no. 3, pp. 1–11, 2020, doi: 10.21008/J.0860-6897.2020.3.02.
3. Fraternali F., Porter M.A., Daraio C.: Optimal design of composite granular protectors, Mech. Adv. Mater. Struct., vol. 17, no. 1, pp. 1–19, Dec. 2009, doi: 10.1080/15376490802710779.
4. Costa D. et al.: Chaos in impact oscillators not in vain: Dynamics of new mass excited oscillator, Nonlinear Dyn., vol. 102, no. 2, pp. 835–861, Oct. 2020, doi: 10.1007/s11071-020-05644-0.
5. Warzecha M., Michalczyk J.: Calculation of maximal collision force in kinematic chains based on collision force impulse, J. Theor. Appl. Mech., vol. 58, no. 2, pp. 339–349, Apr. 2020, doi: 10.15632/jtam-pl/116580.
6. Wang T., Zha X., Chen F., Wang J., Li Y., Jiang F.: Mechanical impact test methods for hard coatings of cutting tools: a review, Int. J. Adv. Manuf. Technol., vol. 115, no. 5–6, pp. 1367–1385, Jul. 2021, doi: 10.1007/s00170-021-07219-8.
7. Nguyen N.S., Brogliato B.:, Multiple Impacts in Dissipative Granular Chains, vol. 72. Berlin, Heidelberg: Springer Berlin Heidelberg, 2014, doi: 10.1007/978-3-642-39298-6.

8. Xie L., Li J., and Liu Y.: Review on charging model of sand particles due to collisions, Theor. Appl. Mech. Lett., vol. 10, no. 4, pp. 276–285, Apr. 2020, doi: 10.1016/j.taml.2020.01.047.
9. Pingle S.M., Fleck N.A., Wadley H.N.G., Deshpande V.S.: Discrete element calculations of the impact of a sand column against rigid structures, Int. J. Impact Eng., vol. 45, pp. 74–89, Jul. 2012, doi: 10.1016/j.ijimpeng.2011.10.005.
10. Zhang Y., Pan G., Zhang Y., Haeri S.: A multi-physics peridynamics-DEM-IB-CLBM framework for the prediction of erosive impact of solid particles in viscous fluids, Comput. Methods Appl. Mech. Eng., vol. 352, pp. 675–690, Aug. 2019, doi: 10.1016/j.cma.2019.04.043.
11. Kakizaki T., Deck J.F., Dubowsky S.: Modeling the spatial dynamics of robotic manipulators with flexible links and joint clearances, J. Mech. Des., vol. 115, no. 4, pp. 839–847, Dec. 1993, doi: 10.1115/1.2919277.
12. Deskiewicz A., Perz R.: Agricultural aircraft wing slat tolerance for bird strike, Aircr. Eng. Aerosp. Technol., vol. 89, no. 4, pp. 590–598, Jul. 2017, doi: 10.1108/AEAT-11-2016-0220.
13. Tenreiro A.F.G., Silva C.M., Lopes A.M., Nunes P.D.P., Carbas R.J.C., da Silva L.F. M.: Design of a new pneumatic impact actuator of a Split Hopkinson Pressure Bar (SHPB) setup for tensile and compression testing of structural adhesives, Mech. Mach. Theory, vol. 159, p. 104289, May 2021, doi: 10.1016/j.mechmachtheory.2021.104289.
14. Jastrzębski D., Perz R.: Rib kinematics analysis in oblique and lateral impact tests, Acta Bioeng. Biomech., vol. 22, no. 1, 2020, doi: 10.37190/ABB-01431-2019-03.
15. Bae D.-M., Prabowo A.R., Cao B., Zakki A.F., Gunawan D.H.: Study on collision between two ships using selected parameters in collision simulation, J. Mar. Sci. Apl., vol. 15, no. 1, pp. 63–72, Mar. 2016, doi: 10.1007/s11804-016-1341-2.
16. Hagiwara K., Takanabe H., Kawano H.: A proposed method of predicting ship collision damage, Int. J. Impact Eng., vol. 1, no. 3, pp. 257–279, 1983, doi: 10.1016/0734-743X(83)90022-2.
17. Flores P.: Contact mechanics for dynamical systems: a comprehensive review, Multibody Syst. Dyn., vol. 54, no. 2, pp. 127–177, Feb. 2022, doi: 10.1007/s11044-021-09803-y.
18. Ghaednia H., Marghitu D.B., Jackson R. L.: Predicting the permanent deformation after the impact of a rod with a flat surface, J. Tribol., vol. 137, p. 011403, Oct. 2014, doi: 10.1115/1.4028709.
19. Daraio C., Nesterenko V.F.: Strongly nonlinear wave dynamics in a chain of polymer coated beads, Phys. Rev. E, vol. 73, no. 2, p. 026612, Feb. 2006, doi: 10.1103/PhysRevE.73.026612.
20. Gharib M., Celik A., Hurmuzlu Y.: Shock absorption using linear particle chains with multiple impacts, J. Appl. Mech., vol. 78, p. 031005, Feb. 2011, doi: 10.1115/1.4003349.
21. Pal R.K., Awasthi A.P., Geubelle P.H.: Characterisation of wave propagation in elastic and elastoplastic granular chains, Phys. Rev. E, vol. 89, no. 1, p. 012204, Jan. 2014, doi: 10.1103/PhysRevE.89.012204.
22. Burgoyne H.A., Daraioand C.: Elastic–plastic wave propagation in uniform and periodic granular chains, J. Appl. Mech., vol. 82, no. 8, p. 081002, Aug. 2015, doi: 10.1115/1.4030458.
23. Daraio C., Nesterenko V.F., Herbold E.B. Jin S.: Energy trapping and shock disintegration in a composite granular medium, Phys. Rev. Lett., vol. 96, no. 5, p. 058002, Feb. 2006, doi: 10.1103/PhysRevLett.96.058002.
24. Jackson R.L., Green I., Marghitu D.B.: Predicting the coefficient of restitution of impacting elastic-perfectly plastic spheres, Nonlinear Dyn., vol. 60, no. 3, pp. 217–229, May 2010, doi: 10.1007/s11071-009-9591-z.
25. Wang H., Yin X., Hao H., Chen W., Yu B.: The correlation of theoretical contact models for normal elastic-plastic impacts, Int. J. Solids Struct., vol. 182–183, pp. 15–33, Jan. 2020, doi: 10.1016/j.ijsolstr.2019.07.018.
26. Ghaednia H., Wang X., Saha S., Xu Y., Sharma A., and Jackson R.L.: A review of elastic–plastic contact mechanics, Appl. Mech. Rev., vol. 69, no. 6, p. 060804, Nov. 2017, doi: 10.1115/1.4038187.
27. Kogut L., Etsion I.: Elastic-plastic contact analysis of a sphere and a rigid flat, J. Appl. Mech., vol. 69, no. 5, pp. 657–662, Sep. 2002, doi: 10.1115/1.1490373.
28. Etsion I., Kligerman Y., KadinY.: Unloading of an elastic–plastic loaded spherical contact, Int. J. Solids Struct., vol. 42, no. 13, pp. 3716–3729, Jun. 2005, doi: 10.1016/j.ijsolstr.2004.12.006.

29. Du Y., Wang S.: Energy dissipation in normal elastoplastic impact between two spheres., J. Appl. Mech., vol. 76, no. 6, p. 061010, Nov. 2009, doi: 10.1115/1.3130801.
30. Brake M.R.: An analytical elastic-perfectly plastic contact model, Int. J. Solids Struct., vol. 49, no. 22, pp. 3129–3141, Nov. 2012, doi: 10.1016/j.ijsolstr.2012.06.013.
31. Deng Q., Yin X.: A comparative study on indentation and flattening contacts, in Proceedings of the 8th International Conference on Fracture, Fatigue and Wear, Singapore: Springer, 2021. Online. Available from: https://doi.org/10.1007/978-981-15-9893-7_4.
32. Brutti C.: A theoretical model for elastic-perfectly plastic flat cylindrical punch indentation, Mech. Mater., vol. 155, p. 103770, Apr. 2021, doi: 10.1016/j.mechmat.2021.103770.
33. Ghaednia H., Mifflin G., Lunia P., ONeill E.O., Brake M.R.W.: Strain hardening from elastic-perfectly plastic to perfectly elastic indentation single asperity contact, Front. Mech. Eng., vol. 6, p. 60, Aug. 2020, doi: 10.3389/fmech.2020.00060.
34. Lee A., Komvopoulos K.: Dynamic spherical indentation of elastic-plastic solids, Int. J. Solids Struct., vol. 146, pp. 180–191, Aug. 2018, doi: 10.1016/j.ijsolstr.2018.03.028.
35. Abirov R. A., Khusanov B.E., Sagdullaeva D.A., Numerical modeling of the problem of indentation of elastic and elastic-plastic massive bodies, IOP Conf. Ser. Mater. Sci. Eng., vol. 971, p. 032017, Dec. 2020, doi: 10.1088/1757-899x/971/3/032017.
36. Electricité de France, Finite element code_aster, Analysis of Structures and Thermomechanics for Studies and Research, 1989.
37. Geuzaine C., RemacleJ.-F.: Gmsh: A 3-D finite element mesh generator with built-in pre- and post-processing facilities: THE GMSH PAPER, Int. J. Numer. Methods Eng., vol. 79, no. 11, pp. 1309–1331, Sep. 2009, doi: 10.1002/nme.2579.